THE ASTROPHYSICAL JOURNAL, 540:1119–1125, 2000 September 10

A 2.5-DIMENSIONAL IDEAL MAGNETOHYDRODYNAMIC MODEL FOR CORONAL MAGNETIC FLUX ROPES[1]

Y. Q. HU AND W. LIU
University of Science and Technology of China, Hefei, Anhui 230026, China
Received 2000 February 10; accepted 2000 April 11

ABSTRACT

Coronal magnetic flux ropes are closely related to various solar active phenomena such as prominences, flares, and coronal mass ejections. Using a 2.5-dimensional (2.5-D), time-dependent ideal MHD model in Cartesian coordinates, a numerical study is carried out to find the equilibrium solution associated with a magnetic flux rope in the corona, which is assumed to emerge as a whole from the photosphere. The rope in equilibrium is characterized by its geometrical features such as the height of the axis, the half-width of the rope, and the length of the vertical current sheet below the rope, and its magnetic properties such as the axial and annular magnetic fluxes and the magnetic helicity as well, which are conserved quantities of the rope in the frame of ideal MHD. It is shown that, for a given bipolar ambient magnetic field, the magnetic flux rope is detached from the photosphere, leaving a vertical current sheet below, when its axial magnetic flux, annular magnetic flux, or magnetic helicity exceeds a certain critical value. The magnetic field is nearly force free in the rope but not in the prominence region, where the Lorentz force takes an important role in supporting the prominence appearing below the rope axis. The geometrical features of the rope vary smoothly with its magnetic properties, and no catastrophe occurs, a similar conclusion to that reached by Forbes & Isenberg for magnetic flux ropes of large radius.

Subject headings: MHD — Sun: corona — Sun: magnetic fields — Sun: prominences

1. INTRODUCTION

Prominences and their eruptions are closely related to solar flares and coronal mass ejections (Tandberg-Hanssen 1974; Priest 1989; Low 1993). Based on observations, prominences have two distinct magnetic configurations, normal and inverse, according to whether their magnetic fields are consistent with or opposite to the photospheric magnetic polarity beneath them (Anzer 1989; Leory 1989). Most prominences have the inverse configuration, and examples of the normal configuration were found only for some low-lying prominences (Leory 1989).

For prominences with the inverse configuration, the oppositely directed magnetic field implies the existence of a magnetic flux rope in the corona. Consequently, the eruption of the magnetic flux rope will naturally cause a prominence eruption, a coronal mass ejection and the associated magnetic flux eruption, and the formation of a vertical current sheet, which leads to solar flares via a fast magnetic reconnection. However, it remains uncertain what the primary mechanism is for the eruption of the magnetic rope. Although the magnetic reconnection was often invoked, many authors suggested that a catastrophic loss of mechanical equilibrium might be responsible for the rope eruption. In terms of a wire current filament model, Van Tend & Kuperus (1978) argued that a loss of equilibrium occurs if the current in the filament exceeds a critical value. An extension of this model was made by Forbes & Isenberg (1991) by including the ideal MHD effect, and they also found that the current filament loses equilibrium if its magnetic energy exceeds a critical value but the filament reaches a new equilibrium with a vertical current sheet below it. Isenberg, Forbes, & Démoulin (1993) made a further extension allowing for a force-free rather than a potential magnetic field within the flux rope, and a similar catastrophic behavior exists for the rope. Lin et al. (1998) used a spherical solar surface and a torus-shaped flux rope that encircles the Sun instead of a flat solar surface and an infinitely long cylindrical flux rope and discussed the effect of the curvature of the flux rope. All these analytical models have assumed that the radius of the flux rope is small compared with the height of the rope axis. The small-radius approximation not only made relevant equilibria analytically tractable but had a subtle implication in the catastrophic behavior of the flux rope. In the model by Forbes & Isenberg (1991), no catastrophe occurs unless the filament radius is smaller than 10^{-3} times the length scale of the photospheric magnetic field. Although the flux-rope radius is allowed to be comparable to the length scale of the photospheric magnetic field in the model by Forbes & Priest (1995), it is still required to be small compared with the height of the rope axis for the validity of the analytical analysis. They also found that the flux-rope radius must be smaller than a certain critical value in order to allow catastrophe to occur.

Numerical simulation studies were also carried out to demonstrate the transition of the flux rope from one equilibrium to another (Forbes 1990) and the ejection of the flux rope driven by fast magnetic reconnection across the newly formed vertical current sheet (Forbes 1991). Magnetic flux-rope models were recently used to explain solar flares (Forbes 1991; Forbes & Priest 1995) and coronal mass ejections (Forbes & Isenberg 1991; Guo, Wu, & Tandberg-Hanssen 1996; Wu & Guo 1999).

Through a careful analysis of the force balance within the prominence, Low & Hundhausen (1995) suggested that a force-free rather than a potential magnetic field must exist in the dark cavity around the prominence and that it carries an electric current of the same sign as the prominence current. The presence of the force-free current makes the O-type neutral point of the resultant magnetic field lie

[1] Major Project 19791090 supported by the National Natural Science Foundation of China.

above the prominence so that no closed field lines lie in their entirety in the prominence. Therefore, the Lorentz force exerted on the prominence current is upward everywhere against gravity, affording the prominence efficient support. If this suggestion is correct, the magnetic flux rope will extend throughout the large-scale cavity, and thus its transverse length scale must be comparable to its height. Moreover, the gravity should be included to construct a more consistent model for the magnetic flux rope.

Lites et al. (1995) made a synthetical analysis of the vector magnetic field measurements, the Hα and magnetogram measurements, and the soft X-ray images of NOAA Active Region 7201 and identified a twisted magnetic flux rope that emerged from the photosphere and entered into the corona, along with the formation and eruption of the associated prominence. Moreover, three-dimensional magnetostatic models were adopted to reasonably explain the observed evolution of the photospheric vector magnetic field (Lites et al. 1995; Lites & Low 1997). In a sense, the interpretation of Lites et al. provided observational evidence for the existence of a magnetic flux rope in the corona and inspired us with the idea that the coronal rope comes from its emergence from the photosphere. Nevertheless, the conclusion on the resultant equilibrium of the coronal rope should be independent of how the rope is initially formed.

In terms of a 2.5-dimensional (2.5-D) ideal MHD model, this paper carries out a numerical study of the dynamic evolution of a magnetic flux rope that emerges from the photosphere and reaches equilibrium in the presence of gravity, with emphasis on the characteristics of the resultant equilibrium associated with the emerged rope and the relationship between the geometrical features and the magnetic properties of the rope.

2. PHYSICAL MODEL AND BASIC EQUATIONS

Coronal magnetic flux ropes are in essence three-dimensional structures. Considering that the length of a magnetic flux rope is generally much larger than its diameter, we use the two-dimensional approximation but allow for the third components of the flow velocity and magnetic field (commonly called 2.5-D models) in this study. Take a Cartesian coordinate system such that the photosphere coincides with the x-z plane and the y-axis is vertical and upward. Introducing a magnetic flux function $\psi(t, x, y)$ related to the magnetic field by

$$B = \nabla \times (\psi \hat{z}) + B_z \hat{z} , \tag{1}$$

the 2.5-D ideal MHD equations may be cast in the nondimensional form

$$\frac{\partial \rho}{\partial t} + v_x \frac{\partial \rho}{\partial x} + v_y \frac{\partial \rho}{\partial y} + \rho \frac{\partial v_x}{\partial x} + \rho \frac{\partial v_y}{\partial y} = 0 , \tag{2}$$

$$\frac{\partial v_x}{\partial t} + v_x \frac{\partial v_x}{\partial x} + v_y \frac{\partial v_x}{\partial y} + \frac{\partial T}{\partial x} + \frac{T}{\rho} \frac{\partial \rho}{\partial x} + \frac{2}{\rho \beta_0} \frac{\partial \psi}{\partial x} \Delta \psi + \frac{2B_z}{\rho \beta_0} \frac{\partial B_z}{\partial x} = 0 , \tag{3}$$

$$\frac{\partial v_y}{\partial t} + v_x \frac{\partial v_y}{\partial x} + v_y \frac{\partial v_y}{\partial y} + \frac{\partial T}{\partial y} + \frac{T}{\rho} \frac{\partial \rho}{\partial y} + \frac{2}{\rho \beta_0} \frac{\partial \psi}{\partial x} \Delta \psi + \frac{2B_z}{\rho \beta_0} \frac{\partial B_z}{\partial y} + g = 0 , \tag{4}$$

$$\frac{\partial v_z}{\partial t} + v_x \frac{\partial v_z}{\partial x} + v_y \frac{\partial v_z}{\partial y} + \frac{2}{\rho \beta_0} \frac{\partial \psi}{\partial x} \frac{\partial B_z}{\partial y} - \frac{2}{\rho \beta_0} \frac{\partial \psi}{\partial y} \frac{\partial B_z}{\partial x} = 0 , \tag{5}$$

$$\frac{\partial \psi}{\partial t} + v_x \frac{\partial \psi}{\partial x} + v_y \frac{\partial \psi}{\partial y} = 0 , \tag{6}$$

$$\frac{\partial B_z}{\partial t} + v_x \frac{\partial B_z}{\partial x} + v_y \frac{\partial B_z}{\partial y} + B_z \frac{\partial v_x}{\partial x} + B_z \frac{\partial v_y}{\partial y} - \frac{\partial v_z}{\partial x} \frac{\partial \psi}{\partial y} + \frac{\partial v_z}{\partial y} \frac{\partial \psi}{\partial x} = 0 , \tag{7}$$

$$\frac{\partial T}{\partial t} + v_x \frac{\partial T}{\partial x} + v_y \frac{\partial T}{\partial y} + (\gamma - 1) T \frac{\partial v_x}{\partial x} + (\gamma - 1) T \frac{\partial v_y}{\partial y} = 0 , \tag{8}$$

where g ($=0.271$ km s$^{-1}/g_0$) is the normalized gravity, β_0 is the characteristic ratio of the gas pressure to the magnetic pressure,

$$\beta_0 = 2\mu_0 \rho_0 R T_0 L_0^2/\psi_0^2 , \tag{9}$$

μ_0 is the vacuum magnetic permeability, R is the gas constant, and ρ_0, T_0, L_0, and ψ_0 are the characteristic values of density, temperature, length, and magnetic flux function, respectively. The characteristic values, i.e., the units of other quantities, may be derived from those defined above, including the velocity $v_0 = (RT_0)^{1/2}$, time $t_0 = L_0/v_0$, magnetic field strength $B_0 = \psi_0/L_0$, acceleration $g_0 = v_0/L_0$, electric current density $j_0 = B_0/(\mu_0 L_0)$, magnetic flux $\Phi_0 = \psi_0 L_0$, electric current intensity $I_0 = j_0 L_0^2$, magnetic helicity $H_0 = \psi_0 B_0 L_0^3$, and so on. As a further simplification, the radiation and heat conduction have been neglected in the energy equation (8).

The initial corona is isothermal and static with

$$T_c \equiv T(0, x, y) = 1 , \quad \rho_c \equiv \rho(0, x, y) = e^{-gy} . \tag{10}$$

The initial magnetic field is assumed to be potential and symmetrical relative to the y-axis. It is produced by two uniform surface magnetic charges at $y = 0$, opposite in sign and located at $-b \le x \le -a$ (negative) and $a \le x \le b$ (positive), respectively (Fig. 1*a*). This potential field can be cast in the complex variable form

$$f(\omega) \equiv B_x - iB_y = \ln\left(\frac{\omega^2 - a^2}{\omega^2 - b^2}\right), \tag{11}$$

where $\omega = x + iy$. The magnetic flux function for the initial magnetic field is then given by

$$\psi_c = \mathrm{Im}\left[\int f(\omega) d\omega\right] = F(a) - F(b) + F(-a) - F(-b) , \tag{12}$$

where

$$F(s) = \frac{1}{2} y \ln[(x - s)^2 + y^2] - (x - s) \arctan\left(\frac{x - s}{y}\right). \tag{13}$$

Figure 1*a* shows the magnetic configuration of the initial magnetic field. It is easy to see that, at $y = 0$, ψ_c is equal to zero for $x \le -b$ and $x \ge b$ and to $(b - a)\pi \equiv \Phi_c$ for $-a \le x \le a$, where Φ_c stands for the total magnetic flux emanating upward from the positive surface charge of unit length along the z-axis. Incidentally, B_z is zero for the initial

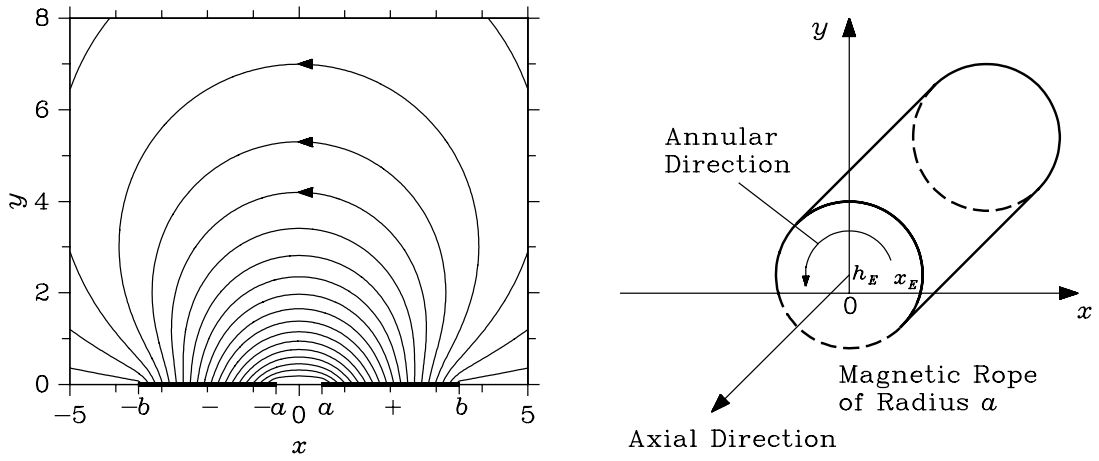

FIG. 1.—Initial magnetic field and a sketch of the emerged rope

magnetic field, and it is confined to the emerged magnetic flux rope, which will be mentioned below.

Assume that a magnetic flux rope of circular cross section begins to emerge at $t = 0$ in the central area of the base and has been fully detached from the photosphere after $t = \tau_E$ (Fig. 1*b*). The radius of the rope is a, and the emergence is uniform. The emerged part of the rope is bounded by $x = \pm x_E$ at time t, where

$$x_E = (a^2 - h_E^2)^{1/2} , \quad h_E = a(2t/\tau_E - 1) . \tag{14}$$

At the base of the emerged part of the rope ($y = 0, |x| \le x_E$) the relevant quantities are specified as a function of t and x as follows:

$$\psi(t, x, 0) = \psi_c(x, 0) + \psi_E(t, x) , \tag{15}$$

$$\psi_E(t, x) = \frac{C_E}{2} \ln\left(\frac{2a^2}{a^2 + x^2 + h_E^2}\right) , \tag{16}$$

$$B_z(t, x, 0) = C_E a(a^2 + x^2 + h_E^2)^{-1} , \tag{17}$$

$$v_y(t, x, 0) = 2a/\tau_E , \quad v_x(t, x, 0) = v_z(t, x, 0) = 0 , \tag{18}$$

$$T(t, x, 0) = 0.02 , \quad \rho(t, x, 0) = 50 , \tag{19}$$

where C_E is a constant and controls the magnetic properties of the emerged rope. The magnetic field given by equations (16) and (17) is a force-free magnetic field of the same form as derived by Gold & Hoyle (1960). Notice that ψ_E given by equation (16) vanishes exactly at $x = \pm x_E$ so that ψ given by equation (15) are continuous there. Besides, $\psi = \Phi_c$ serves as the outer boundary of the emerged rope. A lower temperature and a higher density are specified at the base of the emerged rope during the rope emergence to simulate the cool and dense material within the rope such that the gas pressure is unchanged at the base. After $t = \tau_E$, the state at the base returns to original. A symmetrical condition is used for the left-hand side of the numerical box ($x = 0$), and all the quantities are evaluated by increment equivalent extrapolation on the top and the right-hand side except that B_z is set to be zero and ψ is determined by the condition of zero current ($j_z = -\nabla^2\psi = 0$) there. In the following description, we take the Alfvén transit time $\tau_A = L_0/v_{A0} = (\beta_0/2)^{1/2} t_0$ [$v_{A0} = B_0/(\mu_0 \rho_0)^{1/2}$] as the time unit instead of t_0.

Starting from the initial and boundary conditions, equations (2)–(8) are solved by the multistep implicit scheme (Hu 1989). The computational domain is taken to be $0 \le x \le 5$, $0 \le y \le 12$, and discretized into 52×62 uniform meshes. Relevant characteristic parameters are set to be

$$T_0 = 10^6 \text{ K} , \quad \rho_0 = 3.34 \times 10^{-13} \text{ kg m}^{-3} ,$$

$$\psi_0 = 3.73 \times 10^3 \text{ Wb m}^{-1} ,$$

$$L_0 = 10^4 \text{ km} , \quad a = 0.5 , \quad b = 3.5 , \quad \tau_E = 5\tau_A , \quad \gamma = 5/3 .$$

Consequently, the characteristic values of other quantities are $v_0 = 128.6$ km s^{-1}, $t_0 = 77.8$ s, $v_{A0} = 575$ km s^{-1}, $\tau_A = 17.4$ s, $B_0 = 3.73 \times 10^{-4}$ T, $j_0 = 2.97 \times 10^{-5}$ A m^{-2}, $\Phi_0 = 3.73 \times 10^{10}$ Wb, $I_0 = 2.97 \times 10^9$ A, $H_0 = 1.39 \times 10^{21}$ Wb^2, and so on. Notice that, in order to facilitate the simulation, we have taken a much shorter duration of emergence ($t = 5\tau_A = 87$ s) than observed. Nevertheless, this is immaterial for the analysis below. Actually, it is the magnetic properties of the emerged rope rather than the details of the emergence that determine the equilibrium of the rope in the corona.

3. NUMERICAL RESULTS

Let us first discuss two typical numerical examples, case A and case B, corresponding to $C_E = 8.6$ and 9.5, respectively. For clarity, numerical results are shown in a smaller box: $|x| \le 3$, $0 \le y \le 10$. Figure 2 shows the magnetic field lines at several separate times for the two cases: Figures 2*a*–2*e* for case A and Figures 2*f*–2*j* for case B. After a temporal evolution of $120\tau_A$, the system as a whole approaches quasi-equilibrium for both cases. The magnetic rope sticks to the photosphere for case A (Fig. 2*e*) but breaks away from the photosphere, leaving a vertical current sheet stretching from the photosphere to the bottom of the rope, for case B (Fig. 2*j*). To clearly see the process of approaching quasi-equilibrium, we show in Figure 3 the temporal profiles of h_a, the height of the rope axis (i.e., the O-type neutral point), w, the transverse half-width of the rope, and h_s, the length of the current sheet. For case A (*thick curves*), the current sheet occurs temporarily around $10\tau_A$ but soon disappears; h_a and w smoothly approach their equilibrium values. On the other hand, all these geometrical parameters, especially h_a and h_s, oscillate around their equilibrium values for case B (*thin curves*), with a period about $32\tau_A$ and an amplitude that decays slightly with time.

Figure 4 shows the contours of the density enhancement $\Delta\rho/\rho_c$ [$=(\rho - \rho_c)/\rho_c$], the z-component of the magnetic field B_z, the magnetic helicity density h[$\equiv(\psi - \Phi_c)B_z$; see

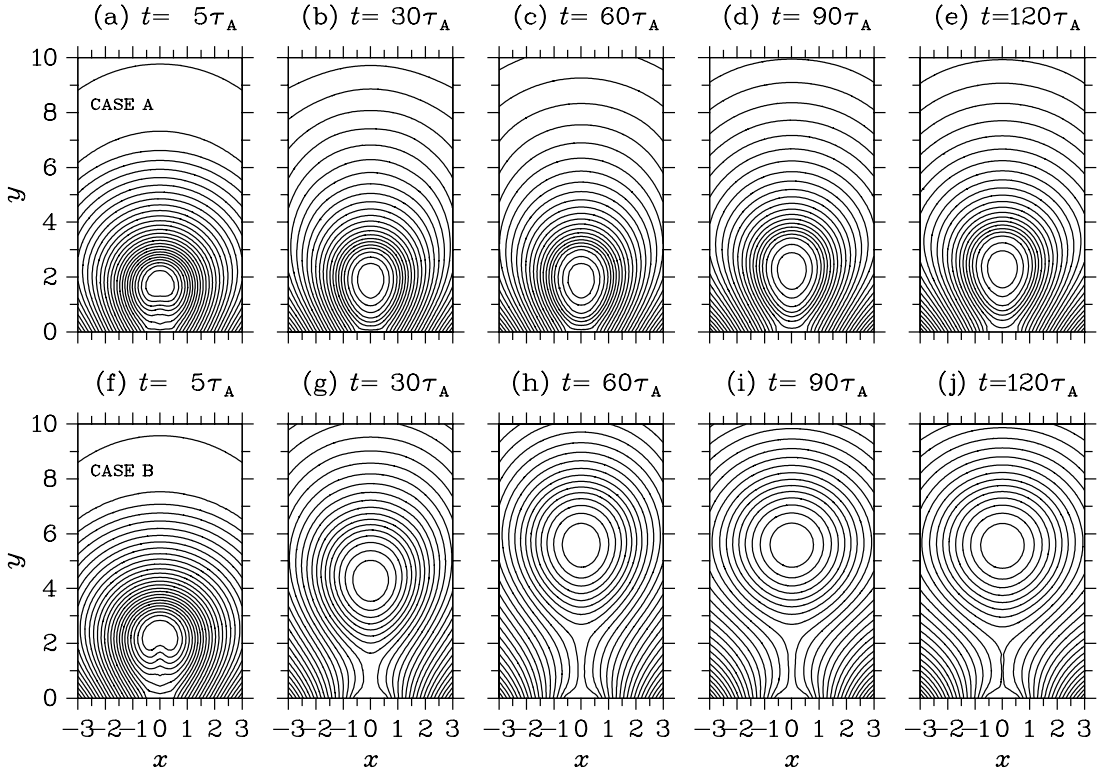

FIG. 2.—Magnetic field lines at several separate times for cases (*a–e*) A and (*f–j*) B

Hu et al. 1997], and the electric current density j by thick curves at $120\tau_A$ for cases A (Figs. 4*a*–4*d*) and B (Figs. 4*e*–4*h*), respectively. The contour levels are uniformly spaced at an interval of 1/10 the peak value given on the top of each panel. For comparison, the corresponding magnetic field lines are also shown by thin-dashed curves in the figure. A high-density region appears below the rope axis, presumably corresponding to the prominence. The total mass within the rope 10 L_0 (10^5 km) in length amounts to 2.64×10^{11} kg for case A and 3.05×10^{11} kg for case B. B_z and h are limited inside the rope, and their contours almost coincide with the magnetic field lines in accord with a vanishing Lorentz force along the z-direction, a necessary condition for 2.5-D equilibrium (cf. eq. [5]). The electric current is mainly distributed within the rope for both cases and in the current sheet for case B as well. Notice that the cross section area of the rope for case B is larger than that for case A because of its rising and expansion, and thus B_z, h, and j become smaller in the rope. The current sheet formed in case B is close to a neutral current sheet where B_z almost vanishes.

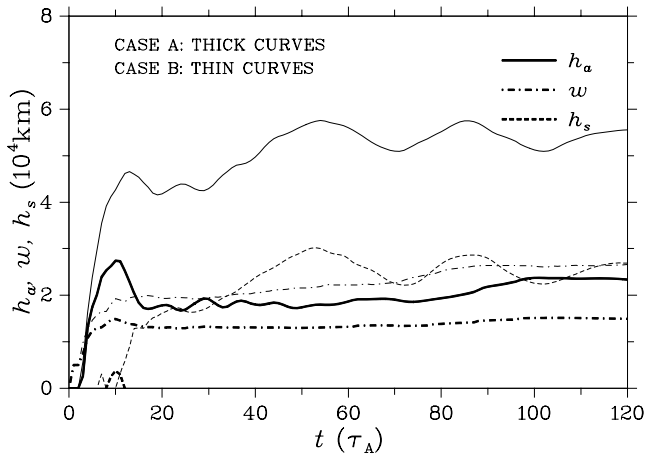

FIG. 3.—Temporal profiles of the height of the rope axis h_a, the transverse half-width of the rope w, and the length of the electric current sheet h_s for cases A and B.

The Lorentz force on the rope current results from a joint action of the repulsion of its image current and the attraction of the photospheric current associated with the initial bipolar field. Initially, the current of the emerged rope is large; the repulsion dominates over the attraction, and the rope rises until it reaches a new equilibrium. The larger the initial current is, the higher the magnetic rope will be for the equilibrium. Figure 5 shows the contours of the vertical component of the Lorentz force density on (Fig. 5*a*) the annular current ($f_{mp} = -j_x B_z$), (Fig. 5*b*) the axial current ($f_{ma} = j_z B_x$), and (Fig. 5*c*) the total currents ($f_m = f_{mp} + f_{ma}$) at $t = 120\tau_A$ for case A. The solid and dotted curves denote positive (upward) and negative (downward) forces respectively, and the thin curves are the field lines. The Lorentz force is distributed within the rope. f_{mp} is upward above and downward below the O-type neutral point, whereas the opposite is true for f_{ma}. f_m almost vanishes outside the prominence, where the magnetic field is close to force free, the same conclusion as reached by Low & Hundhausen (1995). Within most parts of the prominence the Lorentz force on the axial current dominates over that on the annular current so that the net Lorentz force is upward, supporting the prominence. Figure 5*d* shows the net Lorentz force F_m on the whole magnetic rope 10 L_0 in length as a function of time, along with F_{mp} and F_{ma} ($F_m = F_{mp} + F_{ma}$) associated with the annular and axial currents, respectively, and the resultant force F composed of F_m, the

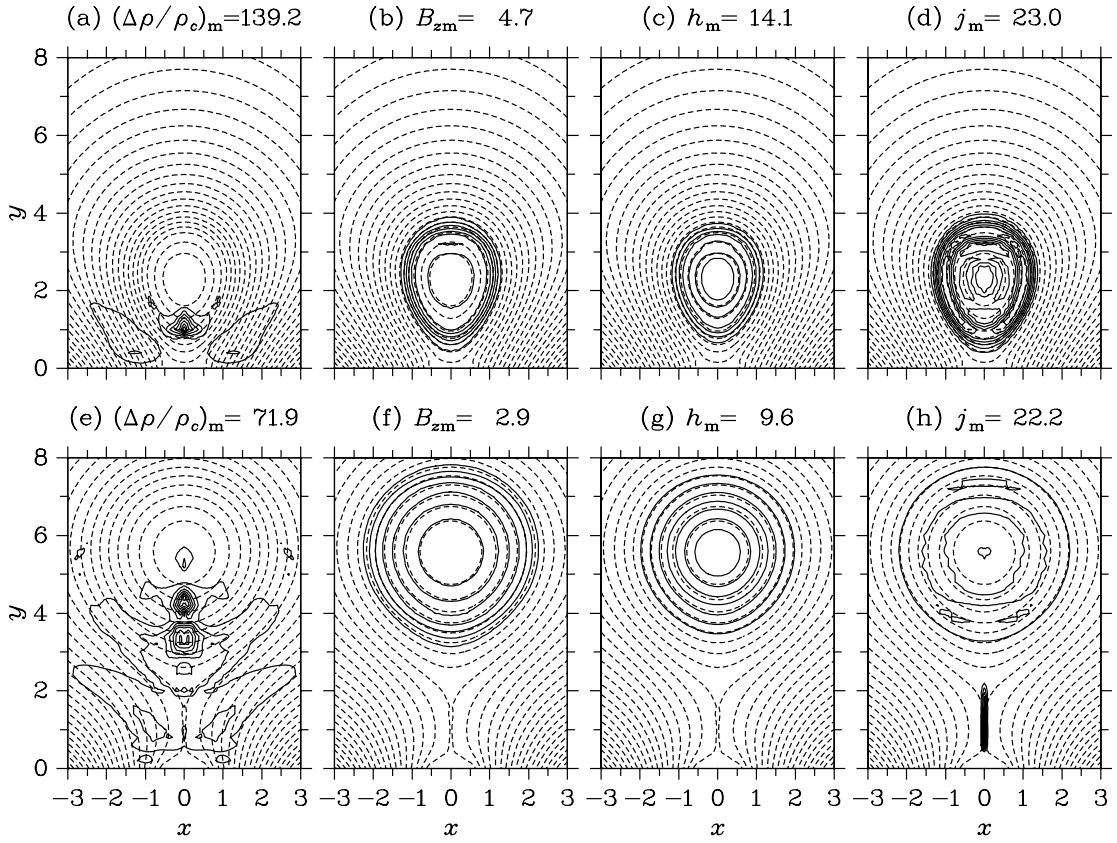

FIG. 4.—Contours of the density enhancement $\Delta\rho/\rho_c$, the z-component of the magnetic field B_z, the magnetic helicity density h, and the electric current density j for cases (*a–d*) A and (*e–h*) B. The contour levels are uniformly spaced with an interval of 1/10 the peak value given on the top of each panel. The dashed curves are the magnetic field lines.

gravitational force, and the gas pressure gradient force. F_{mp} almost vanishes when the equilibrium is reached. This indicates that, in the mechanical equilibrium of the rope, the contribution of the annular current is negligible and the net Lorentz force is entirely attributed to the axial current. This justifies, to some extent, conventional wire filament and small-radius flux-rope models that take only the axial current into account in the analysis of global force balance. In a small region of the upper part of the prominence, the gas pressure gradient force becomes upward and sufficiently large so that the Lorentz force is downward there (see Fig. 5*c*). Incidentally, the resultant force oscillates around zero mainly owing to the oscillation of the Lorentz force with the oscillating rope. Figures 5*e*–5*h* show the corresponding results for case B. Similar conclusions hold true for this case, except that the oscillation in F_m and F is much stronger.

Let us now discuss the influence of the rope emergence parameter C_E (see eqs. [16] and [17]), which determines the magnetic properties of the emerged rope. The related parameters include the axial magnetic flux Φ_z passing through the cross section of the rope, the annular magnetic flux Φ_p of unit length of the rope, that is simply the difference in ψ between the axis and the outer boundary of the rope, the magnetic helicity H of unit length of the rope, the axial current I_z, the annular current I_p of unit length of the rope, and the electric current helicity H_c of unit length of the rope, which is an integration of electric current helicity density ($h_c = j \cdot B$) over the rope cross section. In the frame of ideal MHD, Φ_z, Φ_p, and H are conserved during the temporal evolution of the emerged rope whereas others change during the temporal evolution and approach a steady value after the system reaches quasi-equilibrium. For the two cases mentioned above and other numerical examples to be treated, the maximum relative deviations from conservation between 5 and $120\tau_A$ are within 0.9% for Φ_z, 2.4% for Φ_p, and 1.7% for H, respectively, and the main error source is the numerical dissipation on ψ in the vicinity of the O-type neutral point. Nevertheless, the accuracy is essentially acceptable for our purpose. Owing to the oscillation of the rope around its equilibrium, the three geometrical parameters, h_a, w, and h_s, oscillate with time in varying degrees, whereas the magnetic property parameters mentioned above have no appreciable variations when the quasi-equilibrium is reached. Therefore, we use mean values over an oscillation period for the three geometrical parameters and pick up values at $120\tau_A$ for the magnetic property parameters. As such, these parameters as a function of C_E are obtained and shown in Figure 6. The solid squares, circles, and downward pointing triangles are samples of the numerical results for different values of C_E. The conserved quantities, Φ_z, Φ_p, and H, increase monotonically with increasing C_E (see Figs. 6*b* and 6*d*) as expected, but the nonconserved quantities behave differently. As shown in Figures 6*c* and 6*d*, I_p and H_c decrease monotonically with increasing C_E, whereas I_z first increases with increasing C_E when the rope remains to be attached to the photosphere and then decreases with increasing C_E when the rope breaks away from the photosphere. Actually, the initial values of I_p, H_c, and I_z at $t = \tau_E = 5\tau_A$ are always larger for a larger

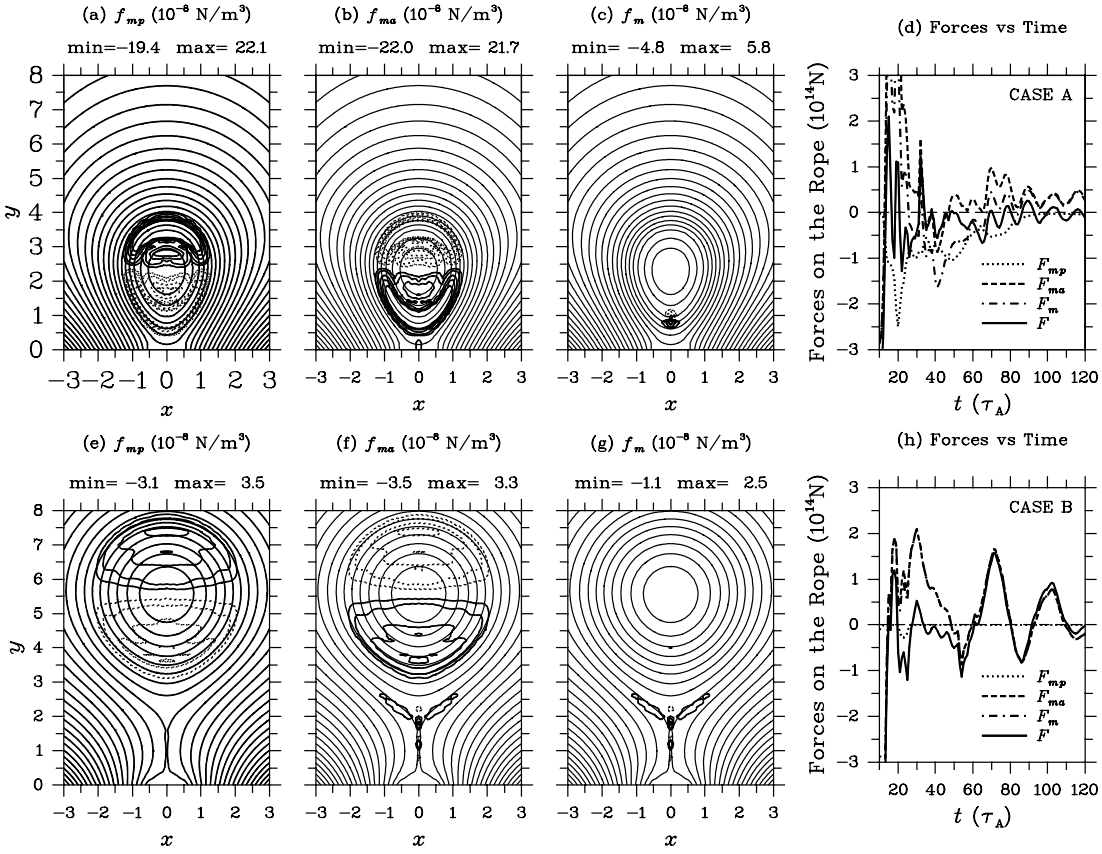

FIG. 5.—Vertical component of the Lorentz force density on the annular current (f_{mp}), the axial current (f_{ma}), and the total current ($f_m = f_{mp} + f_{ma}$) at $t = 120\tau_A$, the vertical Lorentz force on the whole magnetic rope, F_{mp}, F_{ma}, and F_m ($=F_{mp} + F_{ma}$), and the resultant force F vs. time for cases (*a–d*) A and (*e–h*) B. The contour levels of the force density are $\pm(1, 2, 4, 6, 8) \times 10^{-8}$ N m^{-3} in panels *a–c* and $\pm(0.5, 1, 2, 3, 4) \times 10^{-8}$ N m^{-3} in panels *e–g*, positive in solid curves and negative in dotted curves.

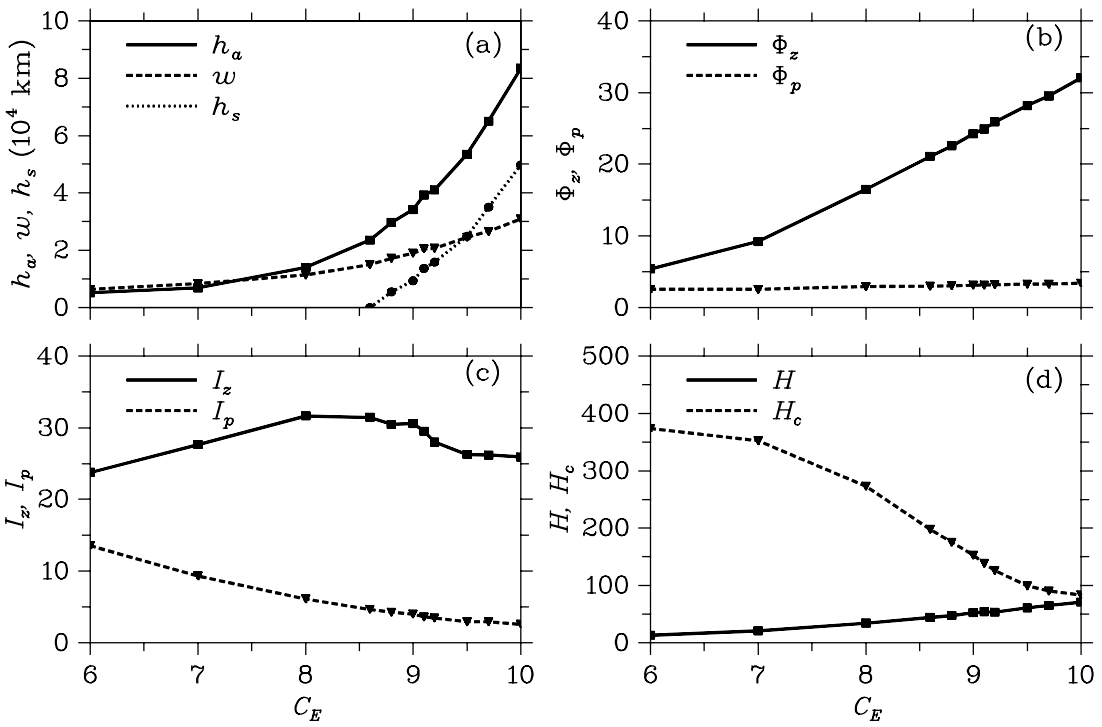

FIG. 6.—Geometrical and magnetic parameters of the coronal magnetic flux rope vs. the rope emergence parameter C_E. The solid squares, circles, and downward-pointing triangles represent the samples of the numerical results.

value of C_E, but these quantities decrease during the temporal evolution of the rope, more substantially for larger values of C_E, and eventually reach their equilibrium values, that are inversely related to C_E for I_p and H_c and also for I_z provided that the rope breaks away from the photosphere.

As seen from Figure 6*a*, the magnetic rope breaks away from the photosphere and a vertical current sheet forms below it when C_E is larger than 8.6. It is interesting that the length of the current sheet, along with the height and half-width of the rope, increases smoothly and monotonically with increasing C_E. Incidentally, if we use the three conserved parameters, Φ_z, Φ_p, and H, instead of C_E, the critical values for the formation of the current sheet are 21, 3.0, and 44, which stand for 7.9×10^{11} Wb, 1.1×10^{11} Wb, and 6.1×10^{22} Wb^2, respectively. While talking about critical values for the three conserved quantities, we do not mean that a current sheet must occur when one of these quantities exceeds the critical value to which we refer above regardless of the values of the other two quantities. As a matter of fact, the behavior of the rope depends on a combination of these conserved quantities. Moreover, the magnetic helicity is related to the axial and annular fluxes for the rope. In terms of the present simple model, the combination is very special, controlled solely by C_E. It is possible to adjust these conserved parameters independently, and it seems that all of them should have a potential influence on the behavior of the rope and the formation of the current sheet. Anyhow, a current sheet must occur if the axial magnetic flux, annular magnetic flux, or magnetic helicity of the rope exceeds a certain critical value.

The profiles shown in Figure 6 may be regarded as a representation of a quasi-static process in which the magnetic properties of the rope change slowly with time through a gradual transfer of magnetic flux and helicity from the photosphere to the rope while maintaining the same distribution of magnetic flux on the photosphere. During this process, the geometrical features of the rope change smoothly with its magnetic properties as seen from Figure 6*a*, so no catastrophe takes place.

4. CONCLUDING REMARKS

Using a 2.5-D ideal MHD model, a numerical study is presented on the coronal response to the emergence of a magnetic rope from the photosphere. The magnetic rope eventually reaches a quasi-equilibrium with or without a vertical current sheet, depending on the magnetic properties of the emerged rope. The numerical results have confirmed the conclusion previously reached by Low & Hundhausen (1995) that the magnetic field within the overlying cavity must be force free and that it plays an important role in efficient support of the prominence. While both the annular and axial currents play equally important roles in maintaining detailed force balance within the rope, the net Lorentz force on the rope as a whole is mainly attributed to the axial current of the rope, whereas the contribution made by the annular current is negligible. We have also explored the relationship between the geometrical features and the magnetic properties of the emerged rope. The geometrical features, including the height and half-width of the magnetic flux rope and the length of the current sheet below the rope, are closely related to the magnetic properties of the rope, represented by the axial and annular fluxes and the magnetic helicity. A current sheet will occur if any of these conserved quantities becomes sufficiently large. The height and the half-width of the rope and the length of the possible current sheet change smoothly with the magnetic properties of the rope, and no catastrophe occurs. This conclusion agrees with that reached by Forbes & Isenberg (1991) for magnetic flux ropes of large radius.

The present simple model has not considered the effect of the ambient magnetic field. A magnetic flux rope should have a higher position in the corona and a longer current sheet below in a weaker ambient magnetic field. Moreover, the photospheric flux function used in this paper is fixed as a smooth function of x in contrast with that associated with two point sources of opposite polarity on the photosphere with a changeable separation, as taken by Forbes & Priest (1995). It will be interesting to test the work of Forbes & Priest starting from a particular solution obtained here with the rope attached to the photosphere and using a photospheric boundary condition close to that taken by Forbes & Priest, and we relegate this task to a future effort. Next, it remains open how each magnetic property of the rope such as the axial and annular fluxes and the magnetic helicity affects the behavior of the rope and the associated current sheet. Finally, a magnetic rope, as a necessary component of the coronal helmet structure, exists stably in the corona for hours and days and then erupts abruptly. This raises a question of the triggering mechanism of such eruption. Photospheric motions, magnetic emergence, and cancellation occurring frequently in active regions may be responsible for the eruption of the magnetic rope and the associated prominence. During these processes magnetic reconnection must play an indispensable role in opening the ambient magnetic field and accelerating the magnetic rope. These issues were treated by previous authors in their own context and are certainly interesting in terms of the present model.

REFERENCES

Anzer, U. 1989, in Dynamics and Structure of Quiescent Solar Prominences, ed. E. R. Priest (Dordrecht: Kluwer), 143
Forbes, T. G. 1990, J. Geophys. Res., 95, 11919
———. 1991, Geophys. Astrophys. Fluid Dyn., 62, 16
Forbes, T. G., & Isenberg, P. A. 1991, ApJ, 373, 294
Forbes, T. G., & Priest, E. R. 1995, ApJ, 446, 377
Gold, T., & Hoyle, F. 1960, MNRAS, 120, 89
Guo, W. P., Wu, S. T., & Tandberg-Hanssen, E. 1996, ApJ, 469, 944
Hu, Y. Q. 1989, J. Comput. Phys., 84, 441
Hu, Y. Q., Xia, L. D., Li, X., Wang, J. X., & Ai, G. X. 1997, Sol. Phys., 170, 283
Isenberg, P. A., Forbes, T. G., & Démoulin, P. 1993, ApJ, 417, 368
Leory, J. L. 1989, in Dynamics and Structure of Quiescent Solar Prominences, ed. E. R. Priest (Dordrecht: Kluwer), 77
Lin, J., Forbes, T. G., Isenberg, P. A., & Démoulin, P. 1998, ApJ, 504, 1006
Lites, B. W., & Low, B. C. 1997, Sol. Phys., 174, 91
Lites, B. W., Low, B. C., Martinez, V., Seagraves, F., & Skumanich, A. 1995, ApJ, 446, 877
Low, B. C. 1993, Bull. Am. Phys. Soc., 38, 2042
Low, B. C., & Hundhausen, J. R. 1995, ApJ, 443, 818
Priest, E. R. 1989, Dynamics and Structure of Quiescent Solar Prominences (Dordrecht: Kluwer)
Tandberg-Hanssen, E. 1974, Solar Prominence (Dordrecht: Reidel)
Van Tend, W., & Kuperus, M. 1978, Sol. Phys., 59, 115
Wu, S. T., & Guo, W. P. 1999, J. Geophys. Res., 104, 14789